Hindawi Publishing Corporation
EURASIP Journal on Advances in Signal Processing
Volume 2011, Article ID 852934, 13 pages
doi:10.1155/2011/852934

Research Article

Adaptive Single Image Superresolution Approach Using Support Vector Data Description

Takahiro Ogawa (EURASIP Member) and Miki Haseyama

Graduate School of Information Science and Technology, Hokkaido University, Sapporo 060-0814, Japan

Correspondence should be addressed to Takahiro Ogawa, ogawa@lmd.ist.hokudai.ac.jp

Received 15 September 2010; Accepted 9 March 2011

Academic Editor: Abdelak Zoubir

An adaptive single image superresolution (SR) method using a support vector data description (SVDD) is presented. The proposed method represents the prior on high-resolution (HR) images by hyperspheres of the SVDD obtained from training examples and reconstructs HR images from low-resolution (LR) observations based on the following schemes. First, in order to perform accurate reconstruction of HR images containing various kinds of objects, training HR examples are previously clustered based on the distance from a center of a hypersphere obtained for each cluster. Furthermore, missing high-frequency components of the target image are estimated in order that the reconstructed HR image minimizes the above distances. In this approach, the minimized distance obtained for each cluster is utilized as a criterion to select the optimal hypersphere for estimating the high-frequency components. This approach provides a solution to the problem of conventional methods not being able to perform adaptive estimation of the high-frequency components. In addition, local patches in the target low-resolution (LR) image are utilized as the training HR examples from the characteristic of self-similarities between different resolution levels in general images, and our method can perform the SR without utilizing any other HR images.

1. Introduction

Estimation of high-resolution (HR) images from low-resolution (LR) images is one of the most important issues in the field of digital imaging applications, and this research field will always be important as long as limitations of hardware and photo environments exist. Nearest neighbor, bilinear, bicubic, and Lanczos-based approaches have been traditionally utilized for enhancing spacial resolutions [1–3]. However, these approaches cannot preserve sharpness at edges and textures in the obtained HR images since the missing high-frequency components cannot be reconstructed.

In order to overcome the limitations of the traditional approaches, super-resolution (SR) methods have been extensively studied by many researchers [1–16]. Most SR methods are broadly categorized into two approaches, reconstruction-based approach and learning-based approach. The reconstruction-based approach estimates the HR image from their multiple LR observations, and many methods based on this approach have been proposed [1–6]. On the other hand, the learning-based (example-based) approach estimates the HR image from only its LR observation, but several other HR images are utilized to learn a prior on the original HR image [8–16]. In this paper, we focus on the learning-based approach and discuss its details.

In order to learn the prior on HR images, many methods adopt multivariate analysis techniques. Principal component analysis (PCA) is frequently utilized for hallucination of face images [17]. Furthermore, kernel PCA (KPCA) is capable of capturing a part of high-order statistics which are particularly important for encoding image structures [18, 19], and the obtained nonlinear eigenspace can successfully represent the priors. Therefore, by utilizing nonlinear subspaces, KPCA-based face hallucination methods have also been proposed [20, 21]. Kim et al. extended this approach to multipatch-based SR of natural images [21].

It should be noted that the conventional approach has the following three problems. (1) In the conventional KPCA-based approach, eigenvectors, which span the nonlinear eigenspace, cannot be directly defined, and the use of the

kernel trick becomes necessary. Thus, even if the dimension of the nonlinear subspace is reduced to a small value, all training examples must be stored for representing this subspace. Problems of memory consumption therefore occur with increase in the number of training examples. (2) In the conventional approach, since several other training HR images must be prepared, suitable training images must be provided manually. (3) The conventional approach is based on the assumption that training examples are globally similar, that is, they should represent a similar class of objects. Therefore, if the target LR image contains several kinds of objects or textures, the performance of the conventional approach tends to be degraded.

Recently, the support vector learning method has become a viable tool in the area of intelligent systems [22]. The support vector machine (SVM) can define its separating hyperplane utilized as a classifier from some support vectors which are selected from training examples. Furthermore, support vector data description (SVDD) [23], whose interest is another type of problem, that is, the problem of data description or one-class classification, can also define its separating hypersphere used as a classifier from only some support vectors.

In this paper, we propose an adaptive single image SR method using SVDD. Since the hypersphere of SVDD can be applied to the data description, we utilize this hypersphere as the subspace of the HR image. As described above, this hypersphere is represented from only some support vectors, and the first problem of the conventional KPCA-based methods can be effectively solved by using SVDD. It is well known that the center of the hypersphere in SVDD is that of the distribution of a target object class. Therefore, from this characteristic, the proposed method regards the hypersphere of SVDD as the subspace of HR images. It should be noted that SVDD, which is a one-class version of SVM, has a characteristic of generalization. Therefore, the proposed method tends to perform accurate reconstruction even if tremendous number of training data cannot be provided. Note that there have been proposed several SR methods which use support vector regression as shown in [24, 25]. These methods utilize the algorithm of SVM, that is, support vector regression for SR. Therefore, their algorithm is based on the regression for estimating HR images. On the other hand, our method uses the hypersphere of SVDD as the subspace of HR images. Then our method adopts entirely different schemes from those conventional methods.

Furthermore, local patches within the target LR image are utilized as HR training examples from a characteristic of self-similarities between two different resolution levels. This means that the training data can be obtained from only the observed image, and the second problem of the conventional methods can be solved. Then, in our method, every patch has potential to be part of the training for individual target patch. This is based on the characteristic of self-similarities as shown in the above. It is well known that general images can be accurately reconstructed from their own self-similarities, and iterated function systems (IFS) [26] effectively use this characteristic. Then, based on the idea of IFS, patches in different resolution levels can be utilized for the accurate reconstruction of images. Therefore, the proposed method also uses the benefit of IFS.

In order to solve the third problem, we introduce the following adaptive classification approach into the estimation of missing high-frequency components in the target image. The proposed method previously performs clustering of training HR local patches based on distances from the center of the hypersphere obtained for each cluster. Furthermore, the high-frequency components minimizing the distances are estimated by using the hypersphere of each cluster. In this procedure, the proposed method monitors the distances minimized in the estimation of the high-frequency components and outputs the results obtained from the optimal cluster minimizing these distances. This classification approach thus enables adaptive estimation of the high-frequency components for each local patch within the target image, and reconstruction of the HR image is realized without dependence on the conventional assumption. Consequently, since the proposed method effectively solves the problems of the conventional methods, successful reconstruction of HR images can be expected.

This paper is organized as follows. In Section 2, the SVDD utilized in the proposed method is explained. In Section 3, the adaptive single image SR method using the SVDD is presented. Experimental results that verify the performance of the proposed method are shown in Section 4. Finally, concluding remarks are presented in Section 5.

2. Support Vector Data Description

In this section, the SVDD utilized in the proposed method is explained. The SVDD was developed by Tax and Duin to solve one-class classification problems [23]. Inspired by the support vector machine learning theory, the SVDD obtains a boundary around the target data set; this boundary is used to decide whether new objects are target objects or outliers.

Given a set of training target data $\mathbf{x}_i$ $(i = 1, 2, \ldots, N)$, the simplest form of the SVDD defines a hypersphere around the data. The sphere is characterized by a center $\mathbf{a}$ and a radius R. The goal is to minimize the volume of the sphere (i.e., minimize R^2) while keeping all training objects inside its boundary. Thus, the following constrained optimization problem must be solved:

$$\begin{aligned} &\min_{R,\mathbf{a},\xi_i} \quad R^2 + T\sum_{i=1}^{N}\xi_i \\ &\text{s.t.} \quad \|\mathbf{x}_i - \mathbf{a}\|^2 \le R^2 + \xi_i, \quad \xi_i \ge 0, \ (i = 1, 2, \ldots, N), \end{aligned} \tag{1}$$

where the parameter T controls the trade-off between the volume and errors, and ξ_i is a slack variable. Then, from the obtained center $\mathbf{a}$ and the radius R, we can decide whether new objects $\mathbf{x}$ are the target objects $\mathbf{P}$ or outliers as follows:

$$\begin{aligned} &\mathbf{x} \in \mathbf{P} \quad \text{if } f_{\text{svdd}}(\mathbf{x}) \ge 0 \\ &\mathbf{x} \notin \mathbf{P} \quad \text{otherwise} \\ &f_{\text{svdd}}(\mathbf{x}) = R^2 - \|\mathbf{x} - \mathbf{a}\|^2. \end{aligned} \tag{2}$$

Figure 1: Relationship between HR image F, blurred HR image $\hat{F}$, and LR image f.

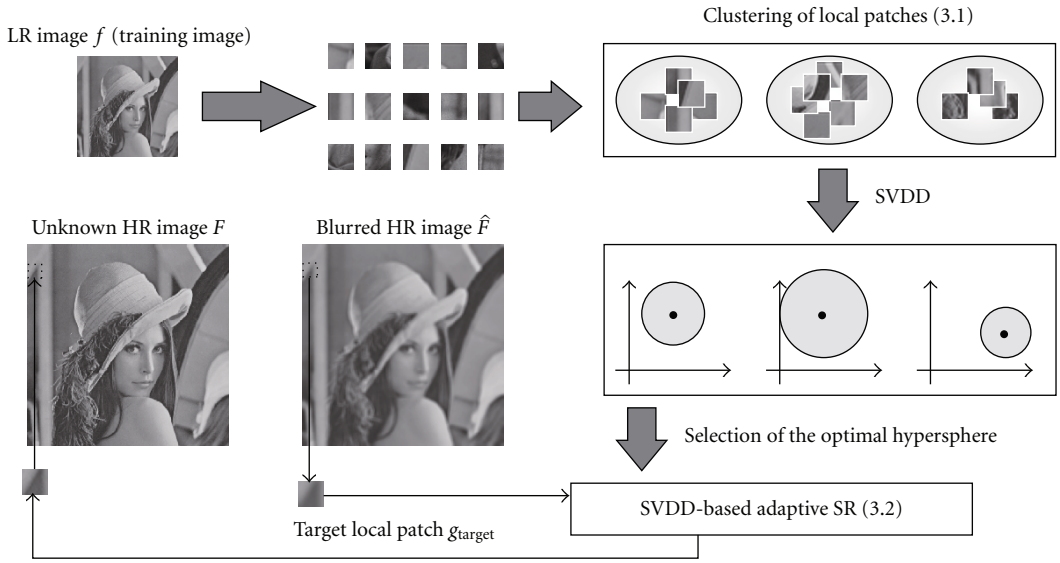

Figure 2: Overview of the adaptive single image SR method based on SVDD.

In the above equation, the output f_{svdd} monotonically decreases with increase in the distance $\|\mathbf{x}-\mathbf{a}\|^2$ between $\mathbf{x}$ and the center $\mathbf{a}$. Therefore, when f_{svdd} becomes larger, $\mathbf{x}$ becomes closer to $\mathbf{a}$. Furthermore, the center $\mathbf{a}$ of the sphere represents that of the probabilistic density for the target objects.

3. SVDD-Based Adaptive SR Method

The adaptive SR method based on the SVDD is presented in this section. As shown in Figure 1, the target LR image f, which we observe, is obtained by blurring and subsampling the HR image F (in this paper, we assume any noises are not included in the target LR image f to make the problem easier.) We can easily calculate the blurred HR image $\hat{F}$ in Figure 1 by upsampling the target LR image f. However, it is difficult to reconstruct F from $\hat{F}$ since the high-frequency components of F are missed by the low-pass filter. Therefore, using the separating hypersphere obtained from training examples by the SVDD, the proposed method tries to estimate the missing high-frequency components. It is well known that local patches between two different resolution levels are similar to each other. Therefore, we utilize local patches within the LR image f for calculating the hypersphere of HR patches. This means the training data can be obtained from only the target LR image f in the proposed method.

It should be noted that in the target LR image f, there are many local patches which are quite different from each other. Such local patches should not affect the estimation of the missing high-frequency components for the target local patch within $\hat{F}$. Therefore, as shown in Figure 2, the proposed method generates the separating hypersphere for each cluster containing similar patches, and the optimal sphere is adaptively utilized for the target local patch in $\hat{F}$. In order to realize this scheme, clustering of the local patches within the target LR image f must first be performed before the high-frequency component estimation of the image $\hat{F}$. Thus, clustering of local patches within the LR image f is explained in Section 3.1, and SVDD-based estimation of the missing high-frequency components is shown in Section 3.2.

3.1. Clustering of Training Local Patches. In this subsection, local patches within the LR image f are clustered into K clusters C^k $(k = 1, 2, \ldots, K)$. First, we clip N local patches f_i ($w \times h$ pixels, $i = 1, 2, \ldots, N$) as the training examples from the target LR image f and generate vectors

$\mathbf{x}_i$ ($i = 1, 2, \ldots, N$), whose elements are their raster scanned intensities. Next, we map $\mathbf{x}_i$ into the feature space to obtain $\phi(\mathbf{x}_i)$ by using the nonlinear map ϕ whose kernel function is the Gaussian kernel [18]. Furthermore, the proposed method assigns f_i to cluster C^k minimizing the following normalized distance:

$$E_i^k = \frac{\left\|\phi(\mathbf{x}_i) - \mathbf{a}^k\right\|^2}{R^{k2}}. \tag{3}$$

In the above equation, $\mathbf{a}^k$ and R^k are the center vector and the radius of the hypersphere obtained from $\phi(\mathbf{x}_j^k)$ ($j = 1, 2, \ldots, N^k$) by the SVDD, where $\phi(\mathbf{x}_j^k)$ represents $\phi(\mathbf{x}_i)$ belonging to cluster C^k. Furthermore, $\mathbf{a}^k$ and R^k are obtained by solving the following optimization problem:

$$\begin{aligned} \min_{R^k, \mathbf{a}^k, \xi_j^k} \quad & R^{k2} + T^k \sum_{j=1}^{N^k} \xi_j^k \\ \text{s.t.} \quad & \left\|\phi(\mathbf{x}_j^k) - \mathbf{a}^k\right\|^2 \le R^{k2} + \xi_j^k, \\ & \xi_j^k \ge 0 \quad \left(j = 1, 2, \ldots, N^k\right), \end{aligned} \tag{4}$$

where the parameter T^k controls the trade-off between the volume and errors, and ξ_j^k is a slack variable. Note that for each cluster, the radius R^k is different since it depends on the features of the belonging local patches. Thus, even if a target object is far from the center $\mathbf{a}^k$ but included in the hypersphere of radius R^k, it should be assigned to cluster C^k. This means simple use of the distance $\|\phi(\mathbf{x}_i) - \mathbf{a}^k\|^2$ may not be suitable for the criterion E_i^k. Therefore, in our method, the normalized distance $\|\phi(\mathbf{x}_i) - \mathbf{a}^k\|^2 / R^{k2}$ is utilized for E_i^k.

In the proposed method, we utilize (3) as the criterion representing how suitable the HR local patch f_i is for cluster C^k. Therefore, we assign each HR training local patch f_i to cluster C^k minimizing this criterion. The calculation of $\mathbf{a}^k$ and R^k is presented in the rest of this subsection.

The constraints in the optimization problem of (4) can be rewritten as follows:

$$\begin{aligned} \left\|\phi\left(\mathbf{x}_j^k\right)\right\|^2 - 2\mathbf{a}^{k\prime}\phi\left(\mathbf{x}_j^k\right) + \left\|\mathbf{a}^k\right\|^2 - R^{k2} - \xi_j^k \le 0, \\ -\xi_j^k \le 0 \quad \left(j = 1, 2, \ldots, N^k\right). \end{aligned} \tag{5}$$

From the above constraints, the Lagrange multipliers for solving the optimization problem in (4) are provided below.

$$\begin{aligned} L^k = {} & R^{k2} + T^k \sum_{j=1}^{N^k} \xi_j^k \\ & - \sum_{j=1}^{N^k} \alpha_j^k \left\{ R^{k2} + \xi_j^k - \left(\left\|\phi\left(\mathbf{x}_j^k\right)\right\|^2 - 2\mathbf{a}^{k\prime}\phi\left(\mathbf{x}_j^k\right) + \left\|\mathbf{a}^k\right\|^2 \right) \right\} \\ & - \sum_{j=1}^{N^k} \beta_j^k \xi_j^k, \end{aligned} \tag{6}$$

where

$$L^k = L\left(R^k, \mathbf{a}^k, \boldsymbol{\xi}^k, \boldsymbol{\alpha}^k, \boldsymbol{\beta}^k\right). \tag{7}$$

In order to solve the optimization problem, we need to maximize the Lagrange multipliers L^k with α_j^k and β_j^k ($j = 1, 2, \ldots, N^k$) and minimize L^k with R^k, $\mathbf{a}^k$, and ξ_j^k. Note that the derivatives of L^k with respect to R^k, $\mathbf{a}^k$, and ξ_j^k become zero at the optimal solution, and

$$\begin{aligned} \frac{\partial L^k}{\partial R^k} &= 0, \\ \frac{\partial L^k}{\partial \mathbf{a}^k} &= 0, \\ \frac{\partial L^k}{\partial \xi_j^k} &= 0, \end{aligned} \tag{8}$$

are satisfied. Therefore, this provides the following equations:

$$\sum_{j=1}^{N^k} \alpha_j^k = 1, \tag{9}$$

$$\mathbf{a}^k = \sum_{j=1}^{N^k} \alpha_j^k \phi\left(\mathbf{x}_j^k\right), \tag{10}$$

$$T^k - \alpha_j^k - \beta_j^k = 0. \tag{11}$$

Then, by substituting (9)–(11) into (6), the following dual problem can be obtained:

$$\begin{aligned} \max_{\alpha_j^k} \quad & \sum_{j=1}^{N^k} \alpha_j^k \kappa\left(\mathbf{x}_j^k, \mathbf{x}_j^k\right) - \sum_{i=1}^{N^k} \sum_{j=1}^{N^k} \alpha_i^k \alpha_j^k \kappa\left(\mathbf{x}_i^k, \mathbf{x}_j^k\right) \\ \text{s.t.} \quad & \sum_{j=1}^{N^k} \alpha_j^k = 1, \quad 0 \le \alpha_j^k \le T^k \ \left(j = 1, 2, \ldots, N^k\right), \end{aligned} \tag{12}$$

where $\kappa(\cdot, \cdot)$ is the Gaussian kernel function, and it satisfies

$$\kappa\left(\mathbf{x}_i^k, \mathbf{x}_j^k\right) = \phi\left(\mathbf{x}_i^k\right)' \phi\left(\mathbf{x}_j^k\right). \tag{13}$$

By solving the optimization problem shown in (12) with respect to α_j^k ($j = 1, 2, \ldots, N^k$), R^{k2} is obtained as follows:

$$\begin{aligned} R^{k2} = {} & \kappa\left(\mathbf{x}_{\text{sv}}^k, \mathbf{x}_{\text{sv}}^k\right) - 2\sum_{j=1}^{N^k} \alpha_j^k \kappa\left(\mathbf{x}_j^k, \mathbf{x}_{\text{sv}}^k\right) \\ & + \sum_{i=1}^{N^k} \sum_{j=1}^{N^k} \alpha_i^k \alpha_j^k \kappa\left(\mathbf{x}_i^k, \mathbf{x}_j^k\right), \end{aligned} \tag{14}$$

where $\mathbf{x}_{\text{sv}}$ is a support vector whose α_j^k satisfies $0 < \alpha_j^k < T^k$. Furthermore, the center vector $\mathbf{a}^k$ of the hypersphere can be obtained from (10).

In this way, iterating the assignment based on (3), the proposed method realizes the clustering of the training HR

(i) A target local patch g_{target} is obtained to calculate the vector $\mathbf{l}$.
(ii) The optimization problem in (15) is solved by (23) for each cluster k ($k = 1, 2, \ldots, K$).
(iii) The criterion E^k in (24) is calculated for each cluster k ($k = 1, 2, \ldots, K$).
(iv) According to the obtained criterion E^k, the following steps are operated for each cluster.
  (a) If $E^k < E^{k'}$ ($k' = \{1, 2, \ldots, K \mid k' \neq k\}$), i.e., E^k of cluster k becomes the minimum value among all classes, $k^{\text{opt}} = k$, and $E^{k^{\text{opt}}}$ and $\hat{\mathbf{x}}^{k^{\text{opt}}}$ are obtained.
  (b) Otherwise, their results are discarded.
(v) From the obtained result $\hat{\mathbf{x}}^{k^{\text{opt}}}$, the following steps are operated.
  (a) If a target pixel has not been reconstructed, the intensity within $\hat{\mathbf{x}}^{k^{\text{opt}}}$ is output.
  (b) If a target pixel has already been reconstructed by other local patches and $E^{k^{\text{opt}}}$ in (iv) is smaller than their results, the intensity is renewed by the result in $\hat{\mathbf{x}}^{k^{\text{opt}}}$.
  (c) Otherwise, the result in $\hat{\mathbf{x}}^{k^{\text{opt}}}$ is discarded.
(vi) Local patches are clipped from $\hat{F}$ in a raster scanning order, and procedures (i)–(v) are iterated.

Algorithm 1: Specific procedures of the high-frequency component estimation in the proposed method.

local patches f_i to K clusters (it should be noted that the initial clusters are simply provided by performing k-means clustering.) Furthermore, by applying the SVDD to each cluster, its hypersphere can be respectively obtained. This hypersphere represents the separating sphere which can decide whether target patches are HR ones or not in each cluster. Therefore, the proposed method utilizes this hypersphere as a subspace of HR images in each cluster. Note that the hypersphere of the SVDD is represented by its center vector $\mathbf{a}^k$ and radius R^k, and these two can be defined from only some support vectors $\mathbf{x}_{\text{sv}}^k$ in each cluster C^k. In detail, α_j^k whose $\mathbf{x}_j^k$ is not the support vector becomes zero by solving the optimization problem in (12). Then $\mathbf{a}^k$ and R^k can be represented by some training HR local patches of the support vectors. Therefore, the hypersphere can also be represented by these training HR patches, and we can effectively solve the problem in the conventional kernel PCA-based approach.

3.2. SVDD-Based Estimation of High-Frequency Components. In this subsection, we explain the SVDD-based method for estimating the missing high-frequency components in $\hat{F}$ from the clustering results obtained in the previous subsection. First, we clip a local patch g_{target} ($w \times h$ pixels) from $\hat{F}$ and obtain a vector $\mathbf{l}$ whose elements are the raster scanned intensities of g_{target}. Furthermore, by using cluster C^k, the proposed method estimates the HR result $\mathbf{x}^k$ of g_{target} by solving the following optimization problem:

$$\max_{\mathbf{x}^k} f_{\text{SVDD}}^k\left(\mathbf{x}^k\right) \quad \text{s.t. } \mathbf{L}\mathbf{x}^k = \mathbf{l}, \tag{15}$$

where $\mathbf{L}$ is the matrix representing the low-pass filter. In our method, a simple sinc filter with a hamming window is utilized. Furthermore, $f_{\text{SVDD}}^k(\mathbf{x}^k)$ is obtained as

$$f_{\text{SVDD}}^k\left(\mathbf{x}^k\right) = {R^k}^2 - \left\|\phi\left(\mathbf{x}^k\right) - \mathbf{a}^k\right\|^2. \tag{16}$$

Then, from the above equation, the optimization problem in (15) can be rewritten as follows:

$$\min_{\mathbf{x}^k} \rho\left(\mathbf{x}^k\right) = \left\|\phi\left(\mathbf{x}^k\right) - \mathbf{a}^k\right\|^2 \quad \text{s.t. } \mathbf{L}\mathbf{x}^k = \mathbf{l}. \tag{17}$$

As shown in the above equation, $\mathbf{x}^k$ is estimated to minimize the distance from the center vector $\mathbf{a}^k$ of the hypersphere for cluster C^k in the feature space. Denoting the vector whose elements are the high-frequency components estimated by cluster C^k as $\hat{\mathbf{h}}^k$, the optimal solution $\hat{\mathbf{x}}^k$ is written as

$$\hat{\mathbf{x}}^k = \mathbf{l} + \hat{\mathbf{h}}^k. \tag{18}$$

Then we find $\hat{\mathbf{h}}^k$ minimizing the following equation under the constraint in (17), and the optimal solution can be obtained.

$$\begin{aligned}\hat{\rho}\left(\mathbf{h}^k\right) &= \left\|\phi\left(\mathbf{l} + \mathbf{h}^k\right) - \mathbf{a}^k\right\|^2 \\ &= \phi\left(\mathbf{l} + \mathbf{h}^k\right)'\phi\left(\mathbf{l} + \mathbf{h}^k\right) + \mathbf{a}^{k\prime}\mathbf{a}^k - 2\phi\left(\mathbf{l} + \mathbf{h}^k\right)'\mathbf{a}^k \\ &= 1 + \mathbf{a}^{k\prime}\mathbf{a}^k - 2\phi\left(\mathbf{l} + \mathbf{h}^k\right)'\mathbf{a}^k.\end{aligned} \tag{19}$$

By using (10), the derivative of (19) with respect to $\mathbf{h}^k$ is obtained as follows:

$$\frac{\partial\hat{\rho}\left(\mathbf{h}^k\right)}{\partial\mathbf{h}^k} = -\sum_{j=1}^{N^k}\frac{4\alpha_j^k}{\theta^k}\left(\mathbf{l} + \mathbf{h}^k - \mathbf{x}_j^k\right)\kappa\left(\mathbf{l} + \mathbf{h}^k, \mathbf{x}_j^k\right), \tag{20}$$

where θ^k is a parameter of the Gaussian kernel. Furthermore, at the extremum of $\hat{\rho}$,

$$\frac{\partial\hat{\rho}\left(\mathbf{h}^k\right)}{\partial\mathbf{h}^k} = 0 \tag{21}$$

is satisfied, and the following equation can be derived:

$$\mathbf{h}^k = \frac{\sum_{j=1}^{N^k}\alpha_j^k\kappa\left(\mathbf{l} + \mathbf{h}^k, \mathbf{x}_j^k\right)\mathbf{x}_j^k}{\sum_{j=1}^{N^k}\alpha_j^k\kappa\left(\mathbf{l} + \mathbf{h}^k, \mathbf{x}_j^k\right)} - \mathbf{l}. \tag{22}$$

Therefore, by renewing $\mathbf{h}_t^k$ in the following equation under the constraint shown in (17), the proposed method enables the calculation of the optimal result $\hat{\mathbf{h}}^k$.

$$\mathbf{h}_{t+1}^k = \frac{\sum_{j=1}^{N^k}\alpha_j^k\kappa\left(\mathbf{l} + \mathbf{h}_t^k, \mathbf{x}_j^k\right)\mathbf{x}_j^k}{\sum_{j=1}^{N^k}\alpha_j^k\kappa\left(\mathbf{l} + \mathbf{h}_t^k, \mathbf{x}_j^k\right)} - \mathbf{l}. \tag{23}$$

(a) (b) (c)

(d) (e) (f)

Figure 3: Subjective performance comparison between the proposed method and the conventional methods (The magnification factor was set to four): (a) original HR image "Lena" (512×512 pixels), (b) LR image (128×128 pixels), (c) HR image estimated by the proposed method, (d) HR image estimated by the interpolation using Lanczos filter, (e) HR image estimated by [10], (f) HR image estimated by [21].

Table 1: Image enlargement performance comparison (SSIM) of the proposed method and the conventional methods (magnification factor = 4).

Test image	LR	Lanczos filter	Reference [10]	Reference [21]	Proposed method
Lena	0.7114	0.8542	0.8168	0.8206	**0.8530**
Goldhill	0.5984	0.7488	0.7133	0.7426	**0.7763**
Peppers	0.7206	0.8449	0.8274	0.8044	**0.8488**
Boat	0.6560	0.7868	0.7500	0.7701	**0.8003**
Girl	0.7831	0.8979	0.8798	0.8809	**0.9039**
Mandrill	0.3900	0.5322	0.4907	0.5478	**0.6008**

Then the estimation result $\hat{\mathbf{h}}^k$ of the high-frequency components by cluster C^k can be calculated, and the HR result $\hat{\mathbf{x}}^k$ of g_{target} is also obtained. The above estimation scheme is similar to the preimage estimation algorithm from the high-dimensional feature space in [27].

Generally, the center $\mathbf{a}^k$ of the separating hypersphere represents that of the probabilistic density for the HR patches in cluster C^k. Therefore, the proposed method estimates $\hat{\mathbf{x}}^k$ of g_{target} in order that it minimizes the distance $\rho(\mathbf{x}^k)$ from the center $\mathbf{a}^k$. Furthermore, if we can classify g_{target} into the optimal cluster $C^{k^{\text{opt}}}$, its high-frequency components can be more accurately estimated by the optimal hypersphere. Thus, we utilize the criterion in (3), and it is defined as

$$E^k = \frac{\left|\left|\phi\left(\hat{\mathbf{x}}^k\right) - \mathbf{a}^k\right|\right|^2}{R^{k\,2}}, \tag{24}$$

and output $\hat{\mathbf{x}}^{k^{\text{opt}}}$ ($k^{\text{opt}} = 1, 2, \ldots, K$) minimizing this criterion as the final result.

As described above, we can reconstruct the HR local patch from g_{target}. The proposed method clips local patches g_{target} ($w \times h$ pixels) at the same interval in a raster scanning

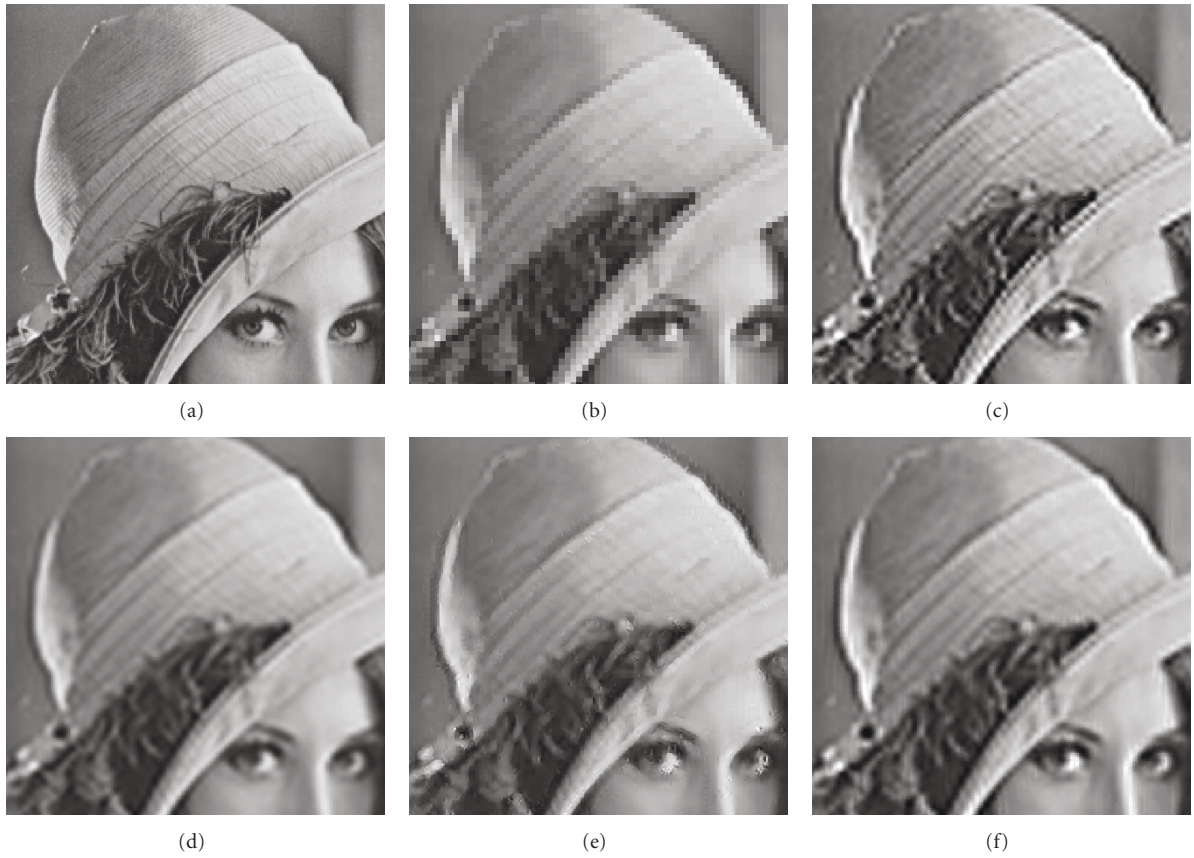

Figure 4: Zoomed portions of the results in Figure 3: (a) zoomed portion of Figure 3(a), (b) zoomed portion of Figure 3(b), (c) zoomed portion of Figure 3(c), (d) zoomed portion of Figure 3(d), (e) zoomed portion of Figure 3(e), and (f) zoomed portion of Figure 3(f).

order from the blurred HR image $\hat{F}$. Furthermore, each local patch is reconstructed by the above schemes. Note that each pixel has multiple estimation results if the clipping interval is smaller than the size of the local patches. In this case, the proposed method regards the result minimizing the criterion in (24) as the final result. Then we can realize adaptive example-based SR of the target LR image. Finally, we show the specific procedures of the high-frequency component estimation in Algorithm 1.

Note that in our method, we only focus on the resolution enhancement of the target LR image. However, the target LR images may be degraded by some blurring effects. If the blur function is included in the degradation process, we have to change the matrix $\mathbf{L}$ in (15) to the matrix including not only the low-pass filter but also the blurring. Specifically, given the matrix $\mathbf{B}$ representing the blurring, (15) is written as

$$\max_{\mathbf{x}^k} f^k_{\mathrm{SVDD}}\left(\mathbf{x}^k\right) \quad \text{s.t. } \mathbf{L}\mathbf{B}\mathbf{x}^k = \mathbf{l}, \tag{25}$$

where $\mathbf{l}$ corresponds to the vector of the target local patch which is also corrupted by the blurring. Then, by solving the above equation, the proposed method can reconstruct the HR image from its LR image degraded by the blurring. It should be noted that in order to realize this reconstruction, we have to perform blur estimation, and it must be provided by some other methods.

4. Experimental Results

The performance of the proposed method is verified in this section. As shown in Figure 3(a), we used a test image "Lena" of 512×512 pixels in size and 8 bits/pixel as an HR image. In order to obtain its LR image, we subsampled this image to 128×128 pixels by using a Lanczos filter as shown in Figure 3(b) (in this figure, we simply enlarge the LR image to the same size of the HR image.) Next, the proposed method was applied to the LR target image to estimate the HR image as shown in Figure 3(c), that is, the magnification factor was set to four (in the subjective evaluation, we set the magnification factor to four. This is because it becomes difficult to identify the difference of the performance between the proposed method and the conventional methods in the figures if the magnification factor is set to two. Thus, the quantitative evaluation of the magnification factor being two is shown in Table 2.) In order to utilize the proposed method, we simply set its parameters as follows: $w = 8$, $h = 8$, $K = 10$, and θ^k $(k = 1, 2, \ldots, K)$ is set to $10^{-3}\times$ the variance for $\|\mathbf{x}_i - \mathbf{x}_j\|^2$ $(i, j = 1, 2, \ldots, N)$. The parameters w and h were determined

Figure 5: Subjective performance comparison between the proposed method and the conventional methods (the magnification factor was set to four): (a) original HR image "Goldhill" (512×512 pixels), (b) LR image (128×128 pixels), (c) HR image estimated by the proposed method, (d) HR image estimated by the interpolation using Lanczos filter, (e) HR image estimated by [10], and (f) HR image estimated by [21].

based on other conventional methods. This means that the proposed method set w and h to the values similar to those of the conventional methods. Next, K should be determined from the number of texture patterns contained within the target image, but it cannot be easily determined. Thus, in the proposed method, we assume that the number of the texture patterns within the target image is less than 10, and K is set to 10. It should be noted that for images including many texture patterns, K must be set to a lager value. Furthermore, θ^k was roughly determined from some preliminary experiments, but it was not always the optimal value for all images. Therefore, in the proposed method, K and θ^k should be adaptively determined from the target LR image. This will be addressed in the future work.

In the proposed method, the number of training patches, N is one of the most important factors for the accurate reconstruction of HR images. However, it is difficult to determine the suitable value of N, and its optimal number will change for each target image. We can guess that the proposed method does not require tremendous number of training examples since the SVDD has a characteristic of generalization. However, if N is too small a value, the performance of the proposed method is not guaranteed, naturally. As described above, since it is difficult to estimate the suitable value of N, we present two approaches for increasing the number of the training examples. In one approach, we downsample the target LR image iteratively, and obtain multiple smaller images to get more training patches. By focusing on the self-similarities in general images, the number of the training examples can be increased, effectively. Furthermore, the other approach is the use of several other LR images which are similar to the target LR image. If we can obtain such LR images, the performance improvement of the proposed method can be expected. This idea is related to the reconstruction-based SR approach. In this approach, the HR image is reconstructed from its multiple LR observations. It should be noted that our method does not utilize unique procedures in the reconstruction-based approach, such as registration, and thus the total procedures are quite different. However, the idea of the use of multiple LR observations for improving the performance of SR is similar. Therefore, if LR images similar to the target LR image can be retrieved from a database, more accurate estimation of the HR image becomes feasible. Note that in this experiment, we did not use the above two approaches since training examples could be sufficiently provided.

For comparison, we respectively show results obtained by the interpolation method using the Lanczos filter, and the

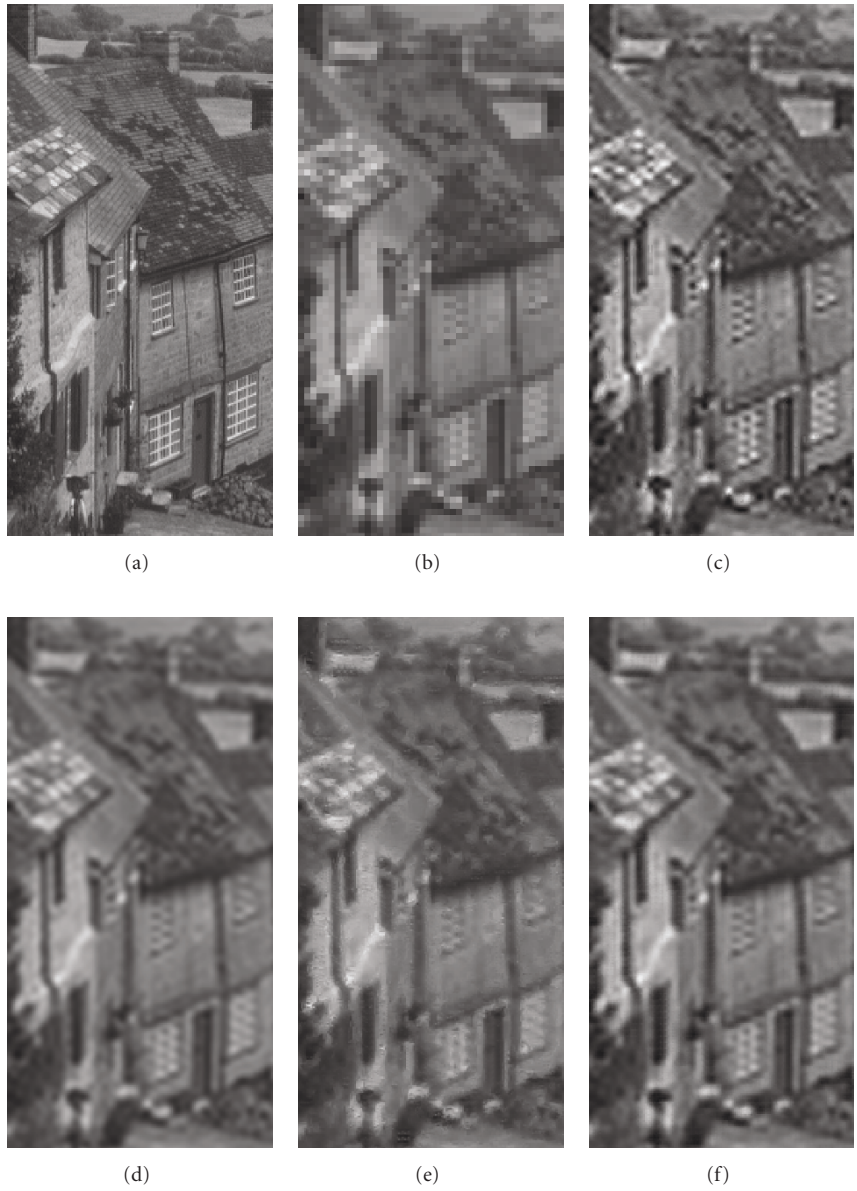

(a) (b) (c)

(d) (e) (f)

Figure 6: Zoomed portions of the results in Figure 5: (a) zoomed portion of Figure 5(a), (b) zoomed portion of Figure 5(b), (c) zoomed portion of Figure 5(c), (d) zoomed portion of Figure 5(d), (e) zoomed portion of Figure 5(e), and (f) zoomed portion of Figure 5(f).

conventional methods [10, 21] in Figures 3(d)–3(f) (in this experiment, we performed the enhancement of the results obtained by our method and the conventional methods for better evaluation. Specifically, the high-frequency components were enhanced by the high-boost filter in the same way as [21].) The conventional method in [10] is a representative method of the example-based SR. Furthermore, the method in [21] is also a representative method which utilizes kernel PCA for obtaining the prior on HR images to perform the SR. Thus, in this experiment, we utilized these conventional methods for the comparison of our method. Note that the conventional methods need other training HR images for estimating missing high-frequency components. In this experiments, we obtain the training data by the same schemes in the proposed method. Furthermore, as shown in Figure 4, we show the zoomed portions of the results obtained by the proposed method and the conventional methods for better subjective evaluation. From the obtained results, we can see that the proposed method preserves the sharpness more successfully than do the conventional methods. Furthermore, we also show the results of "Goldhill" as shown in Figures 5 and 6, where the magnification factor was also set to four. Note that the proposed method performs block-based procedures, and this causes some artifacts at several areas, such as chin of Lena in Figure 3. Other conventional methods also utilize the same procedures, and they also suffer from such artifacts in several areas. Therefore, for all methods adopting the block-based procedures, that

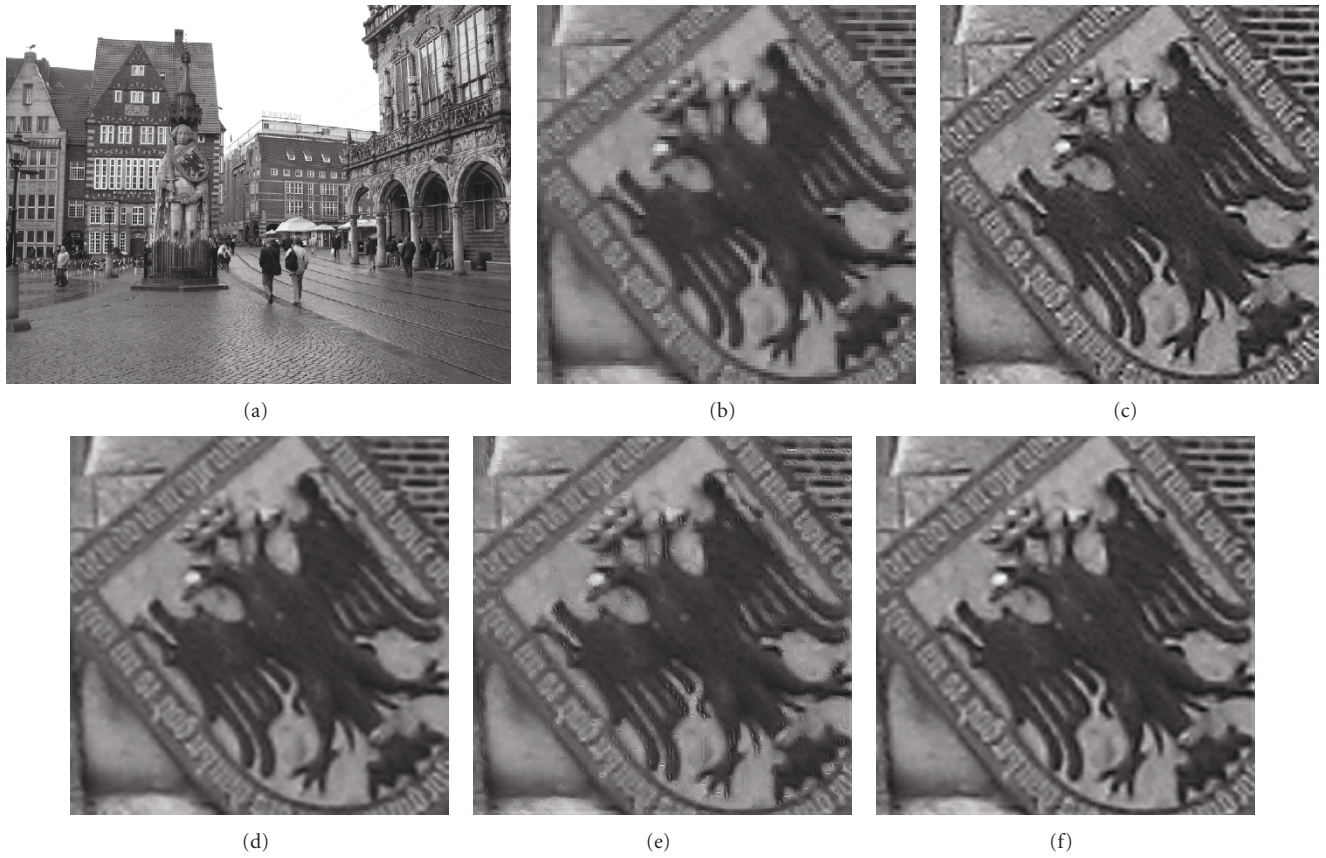

(a) (b) (c)

(d) (e) (f)

Figure 7: Subjective performance comparison between the proposed method and the conventional methods: (a) test image (1600×1200 pixels), (b) LR image (100×100 pixels) clipped from (a), (c) HR image estimated by the proposed method, (d) HR image estimated by the interpolation using Lanczos filter, (e) HR image estimated by [10], and (f) HR image estimated by [21]. The obtained results are 400×400 pixels, that is, the magnification factor is set to four.

is, not only the proposed method but also the conventional methods, several deblocking filters should be used, or some schemes including deblocking effects are necessary.

In order to quantitatively evaluate the performance of the proposed method, we use six test images "Lena", "Goldhill", "Peppers", "Boat", "Girl", and "Mandrill" and performed the same simulations as those for which results are shown in Figures 3–6. It should be noted that the MSE (PSNR) and its variants cannot accurately represent the visual image quality [28, 29]. Therefore, in this experiment, we utilized the SSIM index [30] which is a representative quality measure utilized in many fields of image processing. Tables 2 and 1 show the results of the SSIM index obtained by the proposed method and the conventional methods, where Table 2 is the result of the magnification factor being two, and Table 1 is the result of the magnification factor being four. It can be seen that our method has achieved an improvement over the conventional methods. Therefore, good performance of the proposed method was verified by the experiments.

We discuss the effectiveness of the proposed method. In the KPCA-based method [21], eigenvectors, which span the nonlinear eigenspace, cannot be directly obtained. Thus, even if the dimension of the nonlinear subspace is reduced to a small value, all training examples must be stored for expressing this subspace, and problems of memory consumption occur with increase in the number of the training examples. On the other hand, since the SVDD can also define its separating hypersphere from only some support vectors, the proposed method can effectively solve this problem. Specifically, the ratio of support vectors utilized for representing the hypersphere of each cluster is less than 30% of training examples. Furthermore, the conventional method [21] is based on the assumption that training examples are globally similar, that is, they should represent a similar class of objects. Therefore, if a target LR image contains several kinds of objects, the performance of the conventional approach tends to be degraded. On the other hand, the proposed method monitors the minimized distances in the estimation process of the missing high-frequency components to select the optimal hypersphere utilized for target patches. This approach thus enables adaptive reconstruction of HR images, and successful SR becomes feasible. In addition, our method needs only the target LR image, and we do not have to depend on any other training HR images. Therefore, our method can realize single image SR.

Finally, we show experimental results obtained by applying the proposed and conventional methods to an actual

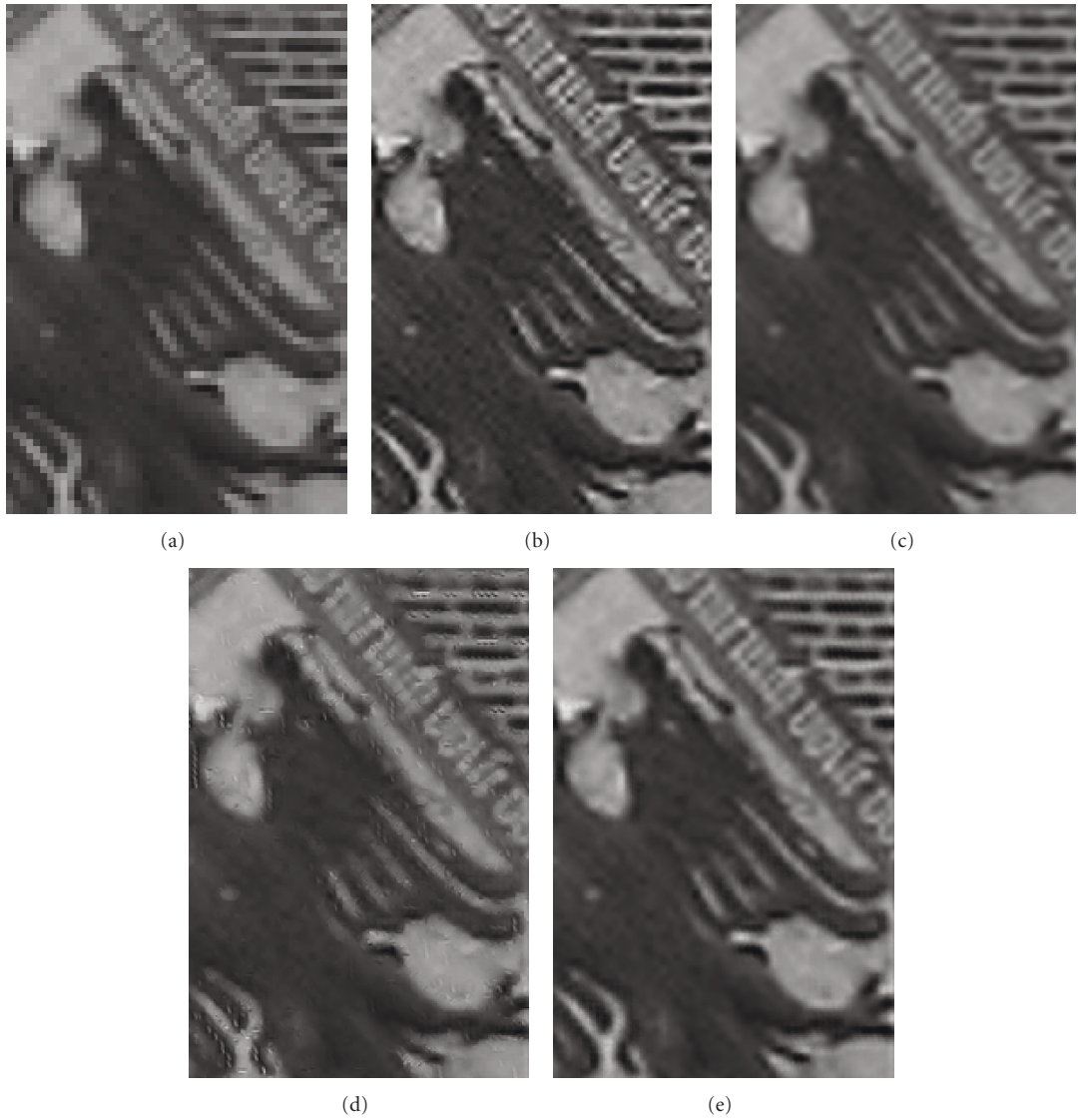

(a) (b) (c)

(d) (e)

Figure 8: Zoomed portions of the results in Figure 7: (a) zoomed portion of Figure 7(b), (b) zoomed portion of Figure 7(c), (c) zoomed portion of Figure 7(d), (d) zoomed portion of Figure 7(e), and (e) zoomed portion of Figure 7(f).

LR image captured from a commercially available camera "Canon IXY DIGITAL 50". It should be noted that the experiments were performed under the same conditions as those shown in the above. From the obtained results shown in Figures 7 and 8, we can see that the proposed method also realizes more successful reconstruction of the HR images than those of the conventional methods. Furthermore, the difference between the proposed method and the conventional methods becomes more significant as the amount of the high-frequency components in the target images becomes larger.

5. Conclusions

An adaptive single image SR method using SVDD is proposed in this paper. In the proposed method, training HR examples are previously clustered, and the separating hypersphere is obtained for each cluster by the SVDD. Note that in our method, local patches in the target LR image are utilized as training examples from the characteristic of self-similarities. Then we can estimate missing high-frequency components minimizing the distances from the center of the hypersphere from only known low-frequency components. Furthermore, the proposed method introduces adaptive selection of the optimal hypersphere into the estimation of the missing high-frequency components by monitoring the minimized distances. This approach enables adaptive estimation of high-frequency components for each local patch within the target image. Therefore, successful reconstruction of HR images can be realized by our SVDD-based method.

Note that the results obtained by the proposed method suffer from some artifacts in high frequency areas. Since our method performs block-based procedures, some blocking

Table 2: Image enlargement performance comparison (SSIM) of the proposed method and the conventional methods (magnification factor = 2).

Test image	LR	Lanczos filter	Reference [10]	Reference [21]	Proposed method
Lena	0.8548	0.9358	0.9348	0.9356	**0.9371**
Goldhill	0.8010	0.8911	0.8872	0.8956	**0.9170**
Peppers	0.8822	0.9509	0.9514	0.9473	**0.9522**
Boat	0.8146	0.8935	0.8899	0.8965	**0.9164**
Girl	0.9072	0.9655	0.9646	0.9665	**0.9641**
Mandrill	0.6551	0.7582	0.7500	0.7720	**0.8265**

artifacts may occur in the regions of block boundaries. Therefore, in future work, we should combine the proposed method and some deblocking filters.

Acknowledgment

This research was partly supported by a Grant-in-Aid for Scientific Research (B) 21300030, from the Japan Society for the Promotion of Science (JSPS).

References

[1] S. C. Park, M. K. Park, and M. G. Kang, "Super-resolution image reconstruction:a technical overview," *IEEE Signal Processing Magazine*, vol. 20, no. 3, pp. 21–36, 2003.

[2] R. Keys, "Cubic convolution interpolation for digital image processing," *IEEE Transactions on Acoustics, Speech, and Signal Processing*, vol. 29, no. 6, pp. 1153–1160, 1981.

[3] A. V. Oppenheim and R. W. Schafer, *Discrete-Time Signal Processing*, Prentice Hall, Upper Saddle River, NJ, USA, 2nd edition, 1999.

[4] S. Baker and T. Kanade, "Limits on super-resolution and how to break them," *IEEE Transactions on Pattern Analysis and Machine Intelligence*, vol. 24, no. 9, pp. 1167–1183, 2002.

[5] S. Farsiu, D. Robinson, M. Elad, and P. Milanfar, "Advances and challenges in super-resolution," *International Journal of Imaging Systems and Technology*, vol. 14, no. 2, pp. 47–57, 2004.

[6] J. D. van Ouwerkerk, "Image super-resolution survey," *Image and Vision Computing*, vol. 24, no. 10, pp. 1039–1052, 2006.

[7] C. V. Jiji, S. Chaudhuri, and P. Chatterjee, "Single frame image super-resolution:should we process locally or globally?" *Multidimensional Systems and Signal Processing*, vol. 18, no. 2-3, pp. 123–152, 2007.

[8] A. Hertzmann, C. E. Jacobs, N. Oliver, B. Curless, and D. H. Salesin, "Image analogies," in *Proceedings of the Computer Graphics Annual Conference (SIGGRAPH '01)*, pp. 327–340, August 2001.

[9] W. T. Freeman, E. C. Pasztor, and O. T. Carmichael, "Learning low-level vision," *International Journal of Computer Vision*, vol. 40, no. 1, pp. 25–47, 2000.

[10] W. T. Freeman, T. R. Jones, and E. C. Pasztor, "Example-based super-resolution," *IEEE Computer Graphics and Applications*, vol. 22, no. 2, pp. 56–65, 2002.

[11] T. A. Stephenson and T. Chen, "Adaptive markov random fields for example-based super-resolution of faces," *EURASIP Journal on Applied Signal Processing*, vol. 2006, Article ID 31062, 11 pages, 2006.

[12] Q. Wang, X. Tang, and H. Shum, "Patch based blind image super resolution," in *Proceedings of the IEEE International Conference on Computer Vision (ICCV '05)*, vol. 1, pp. 709–716, 2005.

[13] X. Li, K. M. Lam, G. Qiu, L. Shen, and S. Wang, "An efficient example-based approach for image super-resolution," in *Proceedings of the IEEE International Conference Neural Networks and Signal Processing (ICNNSP '08)*, pp. 575–580, June 2008.

[14] J. Sun, N. N. Zheng, H. Tao, and H. Y. Shum, "Image hallucination with primal sketch priors," in *Proceedings of the IEEE Computer Society Conference on Computer Vision and Pattern Recognition (CVPR '03)*, vol. 2, pp. 729–736, June 2003.

[15] C. V. Jiji, M. V. Joshi, and S. Chaudhuri, "Single-frame image super-resolution using learned wavelet coefficients," *International Journal of Imaging Systems and Technology*, vol. 14, no. 3, pp. 105–112, 2004.

[16] C. V. Jiji and S. Chaudhuri, "Single-frame image super-resolution through contourlet learning," *EURASIP Journal on Applied Signal Processing*, vol. 2006, Article ID 73767, 11 pages, 2006.

[17] X. Wang and X. Tang, "Hallucinating face by eigentransformation," *IEEE Transactions on Systems, Man and Cybernetics, Part C*, vol. 35, no. 3, pp. 425–434, 2005.

[18] B. Schölkopf, A. Smola, and K. R. Müller, "Nonlinear principal component analysis as a kernel eigen value problem," *Neural Computation*, vol. 10, pp. 1299–1319, 1998.

[19] B. Schölkopf, S. Mika, C. J. C. Burges et al., "Input space versus feature space in kernel-based methods," *IEEE Transactions on Neural Networks*, vol. 10, no. 5, pp. 1000–1017, 1999.

[20] A. Chakrabarti, A. N. Rajagopalan, and R. Chellappa, "Super-resolution of face images using kernel PCA-based prior," *IEEE Transactions on Multimedia*, vol. 9, no. 4, pp. 888–892, 2007.

[21] K. I. Kim, M. O. Franz, and B. Schölkopf, "Iterative kernel principal component analysis for image modeling," *IEEE Transactions on Pattern Analysis and Machine Intelligence*, vol. 27, no. 9, pp. 1351–1366, 2005.

[22] B. Schölkopf and A. J. Smola, *Learning with Kernels: Support Vector Machines, Regularization, Optimization, and Beyond*, MIT Press, Cambridge, Mass, USA, 2002.

[23] D. M. J. Tax and R. P. W. Duin, "Support vector data description," *Machine Learning*, vol. 54, no. 1, pp. 45–66, 2004.

[24] P. M. Goebel and A. N. Belbachir, "Single image superresolution interpolation by wavelet support vector regression," in *Proceedings of the Wavelets and Applications Semester and Conference*, 2006.

[25] K. Ni and T. Q. Nguyen, "Image superresolution using support vector regression," *IEEE Transactions on Image Processing*, vol. 16, no. 6, pp. 1596–1610, 2007.

[26] A. E. Jacquin, "Image coding based on a fractal theory of iterated contractive image transformations," *IEEE Transactions of Image Processing*, vol. 1, no. 1, pp. 18–30, 1992.

[27] S. Mika, B. Schölkopf, A. Smola, K. Müller, M. Scholz, and G. Rätsch, "Kernel PCA and denoising in feature spaces," in *Advances in Neural Information Processing Systems II*, Morgan Kaufman, San Mateo, Calif, USA, 1998.

[28] I. Avcbas, B. Sankur, and K. Sayood, "Statistical evaluation of image quality measures," *Journal of Electronic Imaging*, vol. 11, no. 2, pp. 206–223, 2002.

[29] C. Staelin, D. Greig, M. Fischer, and R. Maurer, *Neural Network Image Scaling Using Spatial Errors*, HP Laboratories, Haifa, Israel, 2003.

[30] Z. Wang, A. C. Bovik, H. R. Sheikh, and E. P. Simoncelli, "Image quality assessment:from error visibility to structural similarity," *IEEE Transactions on Image Processing*, vol. 13, no. 4, pp. 600–612, 2004.